JMEPEG (2014) 23:3459–3466
DOI: 10.1007/s11665-014-1149-7

1059-9495/$19.00

Ni-W Electrodeposited Coatings on Low Carbon Steel Substrate: Fatigue Observations

K.P. Mroz, A. Bigos, S. Kucharski, K. Dolinski, and E. Bełtowska-Lehman

(Submitted March 20, 2014; in revised form June 17, 2014; published online July 15, 2014)

The fatigue response of electrodeposited Ni-W on low carbon steel substrate was studied. The considered Ni-W coatings are a promising substitute for toxic hard chromium coatings which, according to EU directives (2000/53/WE, 2011/37/UE), must be eliminated. Specimens of pure substrate and those covered by coating were compared. Coated specimens exhibited lower fatigue resistance under higher stress amplitudes than their non-coated counterparts in stress-controlled fatigue experiments. However, at lower stress amplitudes, the fatigue strength of both specimen types was similar. The cyclic softening of the coatings was demonstrated using indentation techniques.

Keywords fatigue, hardness, indentation, low carbon steel substrate, Ni-W coatings, S-N curve

1. Introduction

Electrochemical deposition (also known as electrodeposition) is one of the most commonly used techniques for the preparation of adherent metallic coatings used to improve the different properties of the base material (Ref 1). Electrodeposited coatings are not only applied in order to protect the metal substrate from corrosion but also to impart a decorative appearance, enhance wear resistance, improve electrical properties and solderability, etc. (Ref 2, 3). Hard chromium is one of the most widely used coatings in automotive, aerospace, and surface engineering for both decorative and functional purposes. Despite the excellent properties and low manufacturing costs of such coatings, the electrolyte solution employed in their preparation contains toxic hexavalent Cr(VI) ions which, according to EU directives (2000/53/WE, 2011/37/UE), must be eliminated (Ref 4). This declaration has since prompted extensive research aimed at finding an alternative to chromium. Furthermore, it is a well-known fact that hard chromium electroplating decreases the fatigue resistance of a component due to the high residual tensile stress and microcrack density contained in the coating (Ref 5, 6). A promising substitute for such coatings could be nickel-based alloys containing refractory metal (such as Ni-W), which are characterized by high hardness and high wear, thermal, and corrosion resistance (Ref 7, 8). Indeed, many researchers have synthesized nanocrystalline Ni-W alloy to examine a variety of its properties (Ref 9-15). It should be noted, however, that this particular alloy is very difficult to obtain via conventional thermal methods due to the large differences in melting points of the two metals (Ni—1455 °C, W—3410 °C) and their limited mutual solubility. Electrodeposition from aqueous electrolyte solutions (at temperatures lower than 100 °C), a cheap and simple method, is highly suitable for the manufacture of Ni-W coatings, since it enables uniform covering of the substrate surface and simultaneous control over coating thickness and microstructure, thus allowing the design of coating properties.

However, during the electrodeposition of metallic coatings, hydrogen is evolved as a side reaction of the cathode process. This hydrogen may diffuse into the steel lattice (substrate), causing delayed embrittlement when the component is subjected to a load. Although the hydrogen effect taking place during the plating, processes of Zn-Ni and Cd coatings has been investigated by Hillier and Robinson (Ref 16), the amount of hydrogen generated by the coating process has not been well documented. It is a known fact that most of the cracks developing in engineering construction projects result from fatigue processes. The fatigue effect occurs when material is subjected to repeated loading and unloading. If such cyclic loading is above a certain threshold, plastic deformations occur and/or microscopic cracks begin to form at the stress concentrators such as surface/grain interfaces. After cyclic loading, the crack develops to reach a critical size and propagates suddenly, leading to structural failure (Ref 17, 18). Generally, these deformations are irreversible and therefore change the material's stress-strain relationship. Depending on their original state, materials may display cyclic hardening, cyclic softening, or cyclic saturation. Hanlon et al. (Ref 19) found that both fully dense nanocrystalline (13 nm) and ultra fine crystalline (100 nm) Ni produced by electrodeposition exhibited longer stress-controlled fatigue lives compared with that of conventional microcrystalline Ni (1 μm). Based on the results of fatigue crack growth tests, the authors indicated that grain refinement in the nanocrystalline regime can have a deleterious effect on resistance to fatigue fracture. Sriraman et al. (Ref 20) investigated steel samples coated with electrodeposited nanocrystalline Ni-W alloys tested at a maximum stress of 325 MPa, reporting that the samples failed within 3.5×10^5 cycles. In contrast, uncoated specimens tested at the same maximum

K.P. Mroz, S. Kucharski, and **K. Dolinski**, Institute of Fundamental Technological Research, Polish Academy of Sciences, 5b Pawinskiego St., 02-106 Warsaw, Poland; and **A. Bigos** and **E. Beltowska-Lehman**, Institute of Metallurgy and Materials Science, Polish Academy of Sciences, 25 Reymonta St., 30-059 Kraków, Poland. Contact e-mail: kmroz@ippt.pan.pl.

stress did not fail, even after 2.5×10^6 cycles. The authors explained this difference in fatigue behavior as reflecting the presence of tensile residual stresses and inherent microcracks in the coatings which caused an early nucleation of fatigue cracks in the substrate, as also reported by Pertuz et al. (Ref 21) for electroless NiP-coated steels.

The present investigation was undertaken to study the influence of electrodeposited Ni-W on the (S-N) fatigue response of steel samples, one side of which was coated with these alloys. Specimens with and without coating were studied and compared. Both types of specimen were prepared in the same manner in order to investigate the influence of the coatings and the technological process on the fatigue behavior of the elements. Changes in the sample surfaces under loading were monitored using a digital camera with an optical zoom. Broken samples were examined via optical microscopy and indentation techniques to assess the cyclic softening of the coatings.

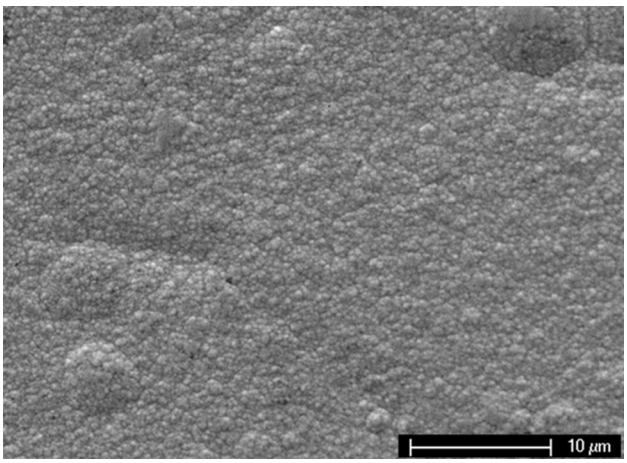

Fig. 1 SEM image of Ni-W (47.7 wt.% W) coating surface electrodeposited at a current density of 5 A/dm^2

2. Experimental Details

2.1 Electrodeposition of Ni-W Coatings

The Ni-W coatings were electrochemically deposited using a well-established process (Ref 8, 22, 23) from sulfate-citrate electrolyte solution containing analytical grade purity chemicals: $NiSO_4 \cdot 7H_2O$, $Na_2WO_4 \cdot 2H_2O$ with a concentration ratio W(VI)/Ni(II) equal to 2 (0.2 and 0.1 M, respectively). Sodium citrate ($Na_3C_6H_5O_7 \cdot 2H_2O$) at a concentration (0.3 M) equal to the sum of the concentrations of the electrodeposited metals was employed as a complexing, buffering, and leveling agent. The pH was adjusted to 8 via the addition of concentrated H_2SO_4 from a starting value of 8.9. No brighteners, detergents, or wetting agents were used. The electroplating of Ni-W coatings was carried out at 60 °C under the galvanostatic regime at 5 A/dm^2, in a system containing a rotating disk electrode (RDE), under constant hydrodynamic conditions corresponding to an RDE rotation speed of 510 rpm. Low carbon steel disks (0.07 dm^2) DC powered by a PAR273A potentiostat/galvanostat were used as a cathode. Prior to each experiment, the steel substrates were degreased, mechanically and chemically polished (in a solution of hydrogen peroxide and oxalic acid at 35 °C), and then rinsed in distilled water in ultrasounds. As an anode, a platinum wire (0.5 dm^2) was used. The obtained metallic, compact and well adherent to the steel substrate Ni-W (47.7 wt.% W) coatings (Fig. 1) were characterized by a nanocrystalline microstructure, with an average grain size of 10 nm.

2.2 Experimental Fatigue

The non-standard specimens were machined from coated disks of radius r = 15 mm; the total thickness of the coated disks was ~2 mm, of which ~10 μm constituted the coating (Fig. 2a). The steel disks (S235JRC cold-drawn) and specimen shape were prepared via electrical discharge machining (EDM)

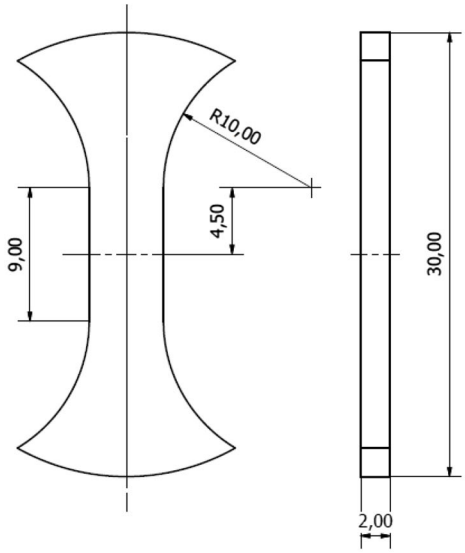

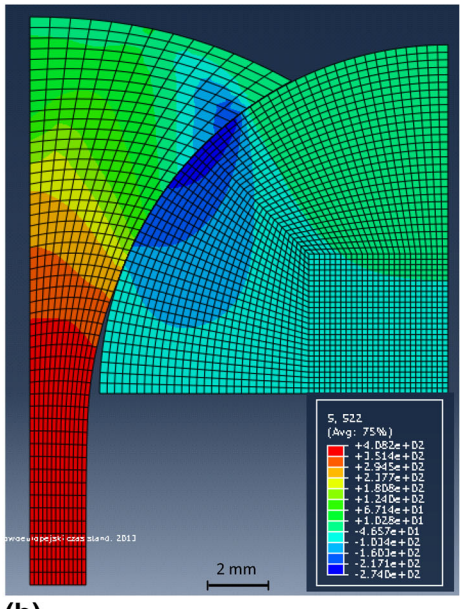

Fig. 2 (a) Specimen geometry, with dimensions in mm; (b) The axial stress distribution σ_{yy} for the employed specimen geometry under monotonic loading, with handle interactions

in a BP-05d (Zap B.P.). Table 1 presents the chemical composition of the base material. Steel mechanical properties were obtained from uniaxial tensile tests, in which yield stress, σ_{YS} = 350 MPa, ultimate tensile strength, σ_{UTS} = 570 MPa, and maximum elongation, ε_f = 16% were reported. These values are typical for the employed steel type and processing method. The shape of the sample was designed with the aim of obtaining a possible uniform distribution of stress in the measuring part, with simultaneous stress concentration (Fig. 2b). The special handle was designed and constructed in order to allow the testing of atypical samples (Fig. 3). Fatigue tests were conducted in an MTS 858 servo-hydraulic fatigue testing machine at a frequency of 10 Hz and at room temperature. Coated specimen fatigue tests were performed in the range from $N = 37 \times 10^3$ cycles to $N = 540 \times 10^3$ cycles, at σ_{max} = 325 to 425 MPa. For the uncoated samples, these values ranged from $N = 120 \times 10^3$ cycles to $N = 460 \times 10^3$ cycles, σ_{max} = 325 to 425 MPa and $R = \sigma_{min}/\sigma_{max} = 0.02$, as presented in Table 2. All experiments were carried out in the controlled load regime using sinusoidal tension loading. The displacement, load, and cycle time were digitally recorded. Changes in the sample surfaces under loading were monitored and recorded by a PCO 1200 HS digital high speed camera with optical zoom. CSM Open Platform equipment was employed to perform Vickers hardness measurements at the microscale. In the microindentation test, the displacement resolution and load resolution were 0.3 nm and 0.1 mN, respectively. To scan the surface of the Ni-W thin layer, a Hommel-Etamic T8000 Nanoscan scanning profilometer was used at a vertical resolution of less than 1 nm.

Table 1 Chemical composition of the substrate, S235JRC

C	Mn	Si	P	S	Cu	N_2
0.13	0.31	0.18	0.009	0.023	0.01	0.005

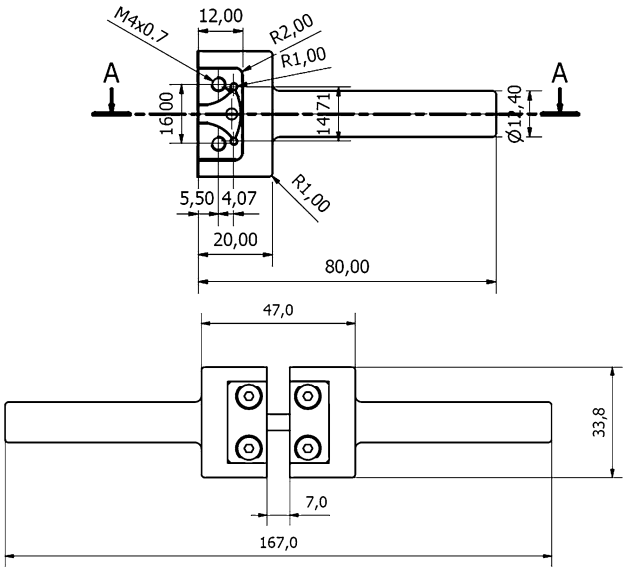

Fig. 3 The handle used in the experiments

3. Results

3.1 Surface Observations

Most frequently, despite the efforts of the manufacturers, the coating was found to contain defects such as pores. Pores (voids) are generally formed irrespective of the substrate preparation method, the plating bath parameters (pH), and the operating parameters of the electrolysis conditions (temperature, hydrodynamic conditions, cathodic current density, and type of anode) as long as the deposition process involves a phase transformation (Ref 24). Porosity reduces macroscopic ductility, since strains are concentrated in the vicinity of the pores, thus reducing the macroscopic tensile strength. Kutzelnigg (Ref 25) has suggested that such pores may be divided into two main categories: transverse pores and masked or bridged pores. Transverse pores may be either hemispherical or channel type and extend through the coating from the basis metal to the surface of the deposit. Masked or bridged pores do not extend through the coating to reach the surface but rather start either at the surface of the basis metal and become bridged or within the coating and become bridged (enclosed pores). One of the many factors affecting porosity is the presence of small non-conducting areas on the substrate. This also seems to be possible for the typical structural steel used in the present investigation. Figure 4 shows the scanning profilometer picture of an unloaded sample, illustrating the transverse and hemispherical pores that extend almost through the entire coating.

The surface topography of the investigated samples is presented in Fig. 5. The height parameters of the surfaces are shown in Table 3, where S_a, S_q, and S_z are the arithmetical mean height, root-mean-square (RMS), and height between the highest peak and deepest valley, respectively. A comparison of the parameters reveals that the roughness of the Ni-W coating is much greater than that of the steel sample. As the steel surface was prepared by polishing and etching, its roughness is mainly an effect of non-conformal grain boundaries. The electrodeposition process does not repeat the roughness of the substrate; instead more wide asperities and valleys are created that could be a source of fatigue cracks. On the other hand, the separated hillocks visible on the Ni-W surface increase the roughness parameters but do not influence fatigue life.

However, the structure of the coating after loading is characteristic. It is well known that under tensile monotonic testing, uniform extension ceases when the tensile load reaches a material-specific maximum. At this point, the test sample

Table 2 Results of the fatigue tests for R = 0.02

(a) For coated specimens												
σ_{max}, MPa	325	325	325	350	350	375	375	400	400	400	425	425
$N \times 10^3$	306	539	249	342	293	121	107	87	122	87	37	80
(b) For non-coated specimens												
σ_{max}, MPa	325	325	325	325	400	400	400	400	425			
$N \times 10^3$	230	361	457	284	199	120	140	133	162			

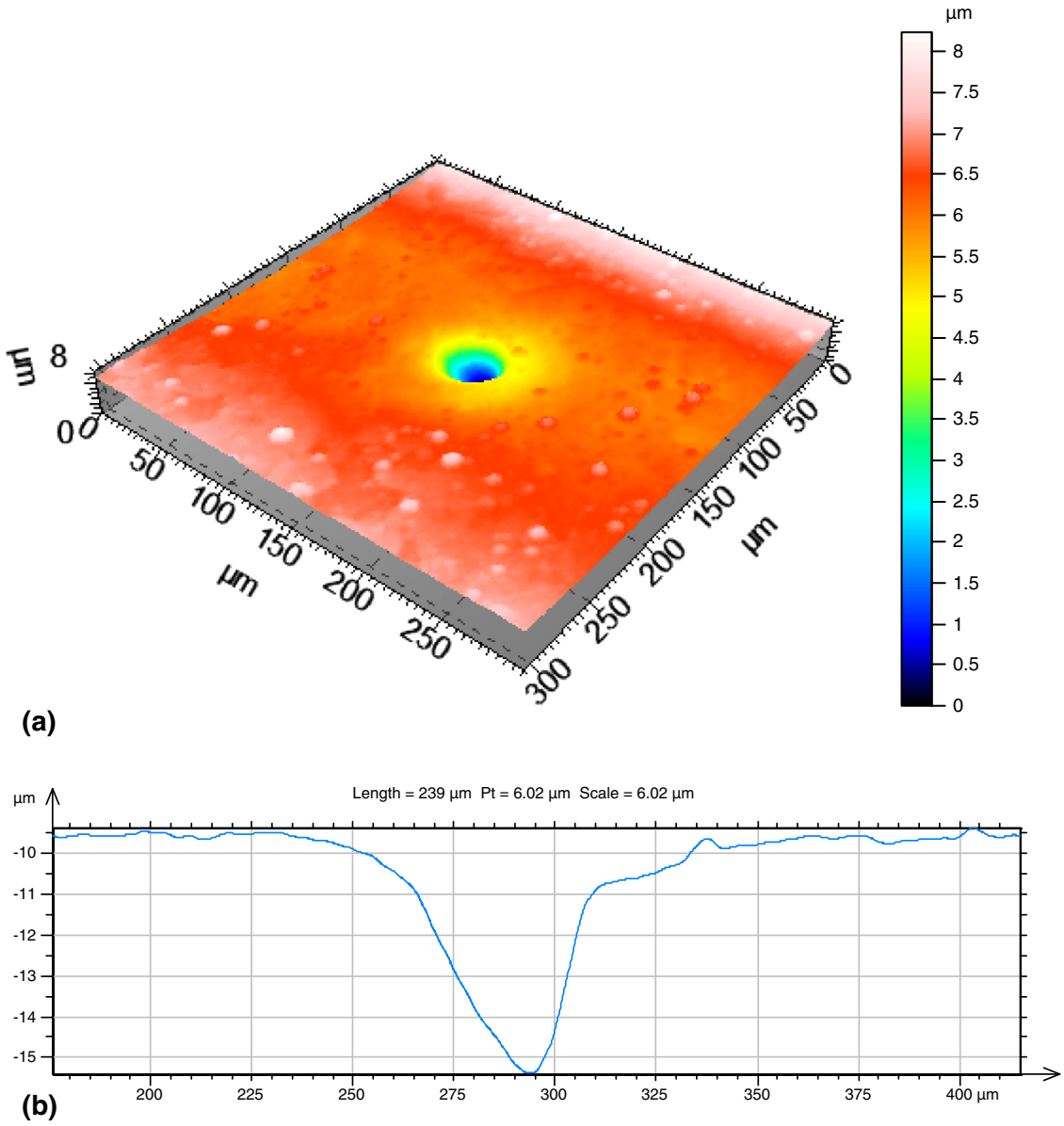

Fig. 4 Measurement of the pores extending through the coating as obtained by the scanning profilometer

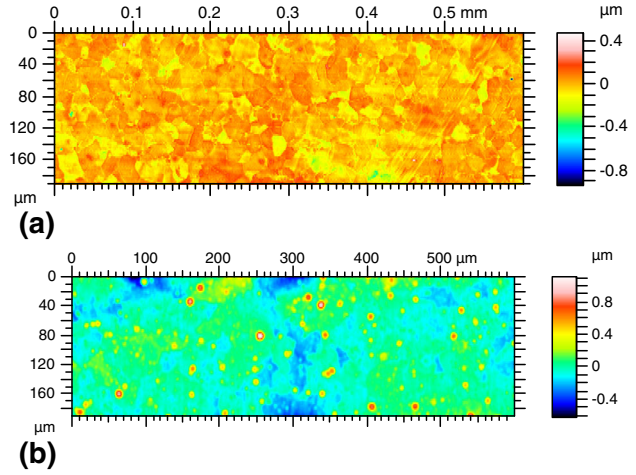

Fig. 5 Example of the surface topography of (a) uncoated and (b) coated specimens obtained via scanning profilometry

Table 3 Surface height parameters

	Coated	Uncoated
S_z	1.74	1.41
S_a	0.0898	0.0539
S_q	0.129	0.0691

begins to neck (Fig. 6a). The state of the stress changes gradually from simple uniaxial tension to a complicated triaxial stress field for a round bar or one of biaxial stress for a thin strip. As a result, the deposited coating is damaged. Generally, the degradation phenomena directly depend on the adhesion and coating strengths. In most cases, delamination at the interface and coating cracking are the main modes of structure degradation. In our case, however, delamination at the interface was seen neither under monotonic nor cyclic loading. Hence, very good adhesion of the deposited coatings might be concluded.

A typical fatigue fracture surface was observed in the present study (Fig. 6b) with the transition from tensile mode (T) to shear mode (S). For the investigated coating, the tensile mode is associated with macroscopic cracking which coincides with a single crack on the surface. No growth of any other defects was recorded in the initial area of fatigue crack propagation (area A). However, with fatigue loading, the coating around the crack tip is gradually damaged, initially by invisible changes of the surface (area B) to net cracking in the forced area (damaged zone), with large plastic deformations.

3.2 Hardness and Young's Modulus

The indentation test is a convenient and sometimes unique method to determine the material properties of thin coatings. One of the most important parameters measured in the indentation test is hardness H, usually interpreted as mean contact pressure. Although many attempts have been made to estimate the constitutive properties of a material on the basis of hardness measurements, the problem remains unsolved and there is no generally accepted method employed to obtain the values of yield strength and tensile strengths using such measurements. The fundamental experimental investigations of material hardness were performed by Tabor (Ref 26) and Johnson (Ref 27). Numerical simulation of indentation tests with sharp indenters was presented in a series of papers by Giannakopoulos and Larsson (Ref 28-30). An exhaustive report concerning a correlation between the hardness and tensile strength of steels is presented in (Ref 31). In the sharp indentation test, three levels can be distinguished that depend on the amount of plastic deformation generated in the vicinity of the imprint and that are pertinent to different indentation responses. These levels can be distinguished using the parameter Γ as follows:

$$\Gamma = \frac{E \tan \beta}{(1 - \nu^2)\sigma_y}, \quad \text{(Eq 1)}$$

where σ_y is the flow stress by the first yield, β is the angle between the sharp indenter and the undeformed surface, and E is the Young's modulus. The general formula for hardness is

$$H = C\sigma_r \quad \text{(Eq 2)}$$

where σ_r is a stress value higher than σ_y (for strain-hardening materials) which corresponds to a certain representative value of plastic strain ε_r.

At level III, in which plastic deformation is present in the whole contact area, the value of C has been estimated by Tabor (Ref 26) as $C \approx 3$, with $\varepsilon_r = 8\%$, although these values were

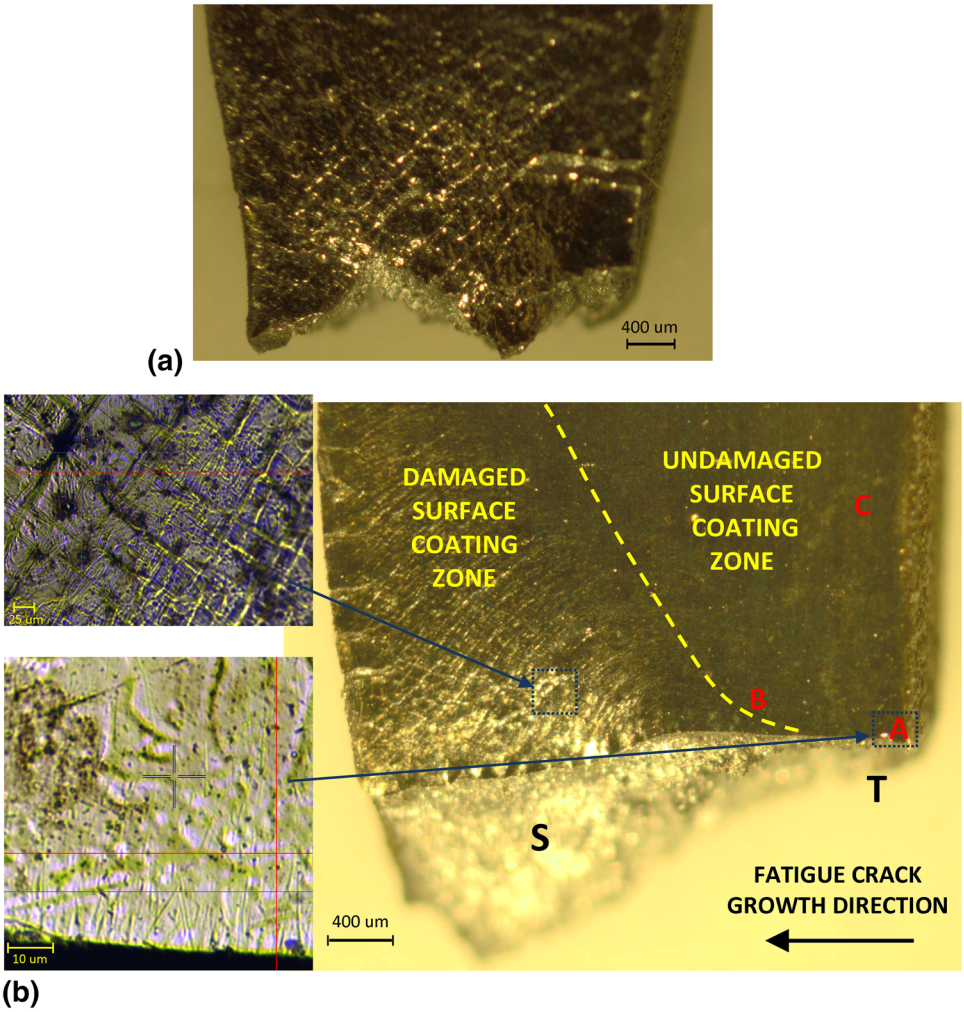

Fig. 6 Fracture surface after (a) monotonic loading and (b) cyclic loading

later corrected to 2.54 and 11%, respectively. The latter values have also been confirmed via numerical analysis (Ref 30) for perfectly plastic materials. Johnson (Ref 27) has suggested that for level II of the indentation test the following formula would be valid

$$H = \frac{2}{3}\sigma_r\left(1 + \ln\frac{E\tan\beta}{3(1-\nu^2)\sigma_y}\right). \quad \text{(Eq 3)}$$

On the basis of numerical analysis (Ref 28, 29), it has been stated that

$$H = 0.29\sigma_y\left(1 + \frac{\sigma_r}{\sigma_y}\right)\left(1 + \ln\frac{E\tan\beta}{3\sigma_y}\right). \quad \text{(Eq 4)}$$

where σ_r corresponds to 30% of plastic strain.

Using the above formulae and taking into account the fact that the analyzed layer exhibited moderate strain hardening (with neither pile-up nor think-in around the imprint), the yield stress of the layer can be estimated at around 3500-4200 MPa. Another estimation formula proposed in (Ref 31),

$$\sigma_y = -90.7 + 2.876H_V \quad \text{(Eq 5)}$$

produces σ_y = 2450 MPa for unstressed damaged specimens, where the yield stress is in MPa and H_V is diamond pyramid hardness in (kgf/mm^2). In both estimation methods, the yield stress of the layer is much higher than that for the steel substrate determined in the tension test.

Under cyclic loading, softening processes are observed in the coating, as demonstrated using the employed indentation techniques. Table 4 and Fig. 7 present hardness values for certain areas of the broken specimen, with data for undamaged specimens, depicted as area D in Table 4, determined for comparison. The highest hardness value (not taking into account undamaged specimen D) and thus also the lowest level of softening, appears in area C, which is relatively far from the final fracture. Next to area C is area A, which is likely associated with initial crack growth and relatively small damage ahead of the crack tip. The lowest hardness and highest softening levels are found in area B (Fig. 6). All recorded changes in the Young's modulus are relatively small.

Table 4 Mean values of coating hardness and Young's modulus in the respective localizations

Area	*H*, MPa	*E*, GPa
B	7805	192
A	8095	196
C	8777	209
D	8975	198

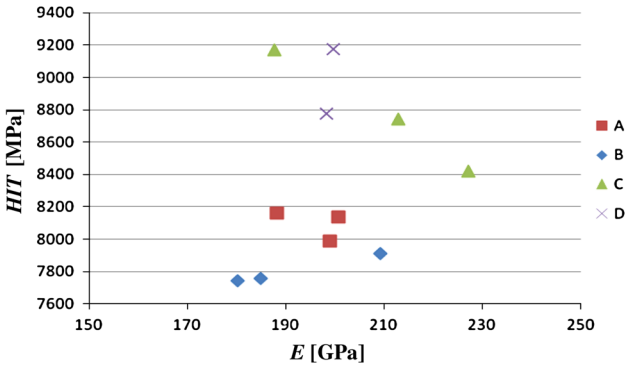

Fig. 7 Indentation hardness and Young's modulus

3.3 Fatigue Loading Results

As mentioned above, during the electrodeposition of metals, the hydrogen interacts with the surface of the substrate, negatively influencing the fatigue behavior of the elements. However, steel substrates are usually prepared for deposition via the use of mechanical and chemical polishing to improve the fatigue properties compared with those obtained by machining. Similarly, cutting via EDM also introduces an improvement in mechanical properties compared with those produced by other cutting methods. Generally, careful preparation of the substrate surface appears very important for the minimization of certain negative effects associated with the coating deposition method on element fatigue strength.

The conducted experiments have shown that the fatigue strength of the electrodeposited coating is dependent on the value of the applied stress amplitude. During the stress-controlled fatigue experiments, coated specimens exhibited a lower fatigue resistance than their non-coated counterparts at higher stress amplitudes. However, at lower stress amplitudes, the fatigue strength of both types of specimen was similar (Fig. 8).

Figure 9 and 10 display examples of crack initiation and propagation at σ_{max} = 400 MPa and σ_{max} = 425 MPa, respectively. At σ_{max} = 400 MPa, the coating damage process started around a surface defect in the middle of the specimen at ~2.5% N_f, where N_f is the number of cycles until final fracture. However, for another identically loaded sample, the number of cycles until the initiation of surface damage differed considerably. Such a discrepancy is obviously related to the randomness of the size and location of each defect.

Nevertheless, the fatigue process always started at macroscopic surface defects in the middle of each specimen, with the development of the dominant crack commencing only at ~60% N_f on the specimen edge. From ~77% N_f the cracks merged to constitute one main crack. Afterward and until the final fracture at N_f = 87000, no visible changes were observed on the rest of the coating surface. The similar nature of the fatigue process for a specimen loaded with σ_{max} = 425 MPa can be seen in Fig. 10. In contrast, for specimens loaded with $\sigma_{max} < 400$ MPa, fatigue damage started on the edge of the samples, with no damage to the coating surface in the middle of the specimen.

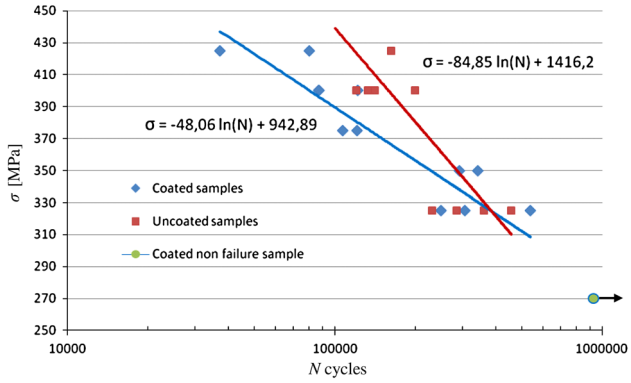

Fig. 8 S-logN data

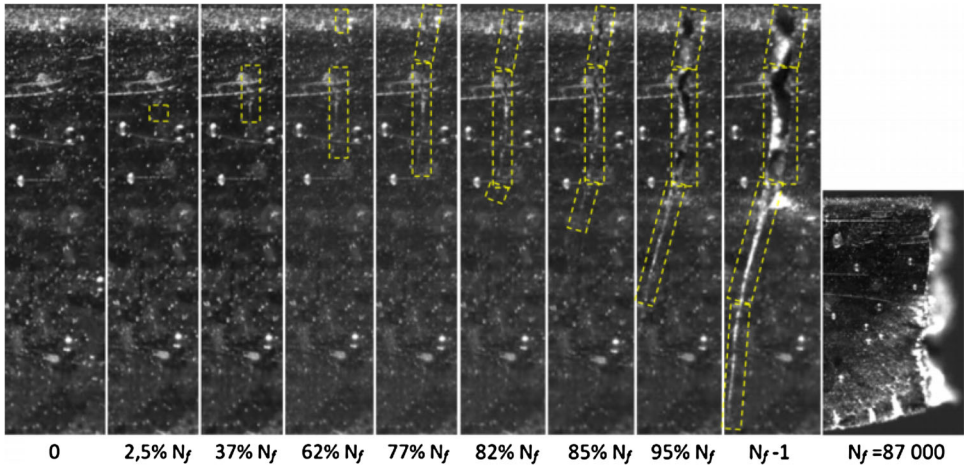

Fig. 9 Fatigue crack initiation and propagation at σ_{max} = 400 MPa, R = 0.02

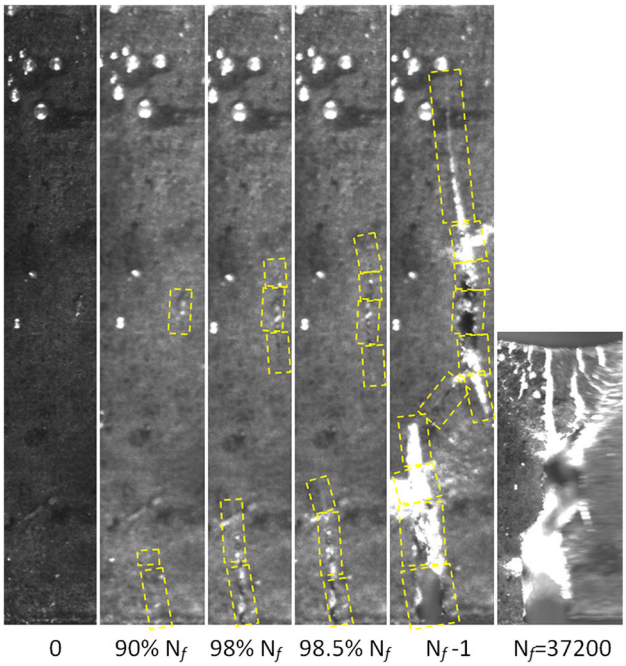

Fig. 10 Fatigue crack initiation and propagation at σ_{max} = 425 MPa, R = 0.02

This pattern might reflect the competition between coating defects and the effect of sample edges, while either is usually the location of fatigue crack initiation. The high yield stress of the coating layer compared with that of the steel substrate makes surface defects less significant (active) than the effects of the substrate edge and/or imperfections in terms of initiating crack formation under small load values.

4. Conclusions

Specimens of low carbon steel, both uncoated and coated with an electrodeposited Ni-W alloy, were investigated, with the different fatigue properties of the coated and uncoated specimens demonstrated. Stress-controlled fatigue experiments revealed that the coated specimens exhibited lower fatigue resistance at higher stress amplitudes than their uncoated counterparts. This should be taken into account when such coated elements are to be used in applications in which intense cyclic loading would be expected. At lower stress amplitudes, the fatigue strength of both types of specimen was similar.

Cyclic softening as a result of fatigue damage was demonstrated using indentation techniques, with the degree of softening found to be directly related to the developmental stage of specimen failure damage, as well as to the relative mutual localization of the investigated area and dominant crack. The most intense softening was measured ahead of the crack tip, in the transition area between tensile mode and shear mode.

It was also found that the coating damage process for samples loaded with $\sigma_{max} \geq 400$ MPa commenced around a surface defect in the middle of the specimen. However, the development of a dominant crack started later on the edge of the specimen. For specimens loaded with $\sigma_{max} < 400$ MPa, fatigue was associated with the growth of the dominant crack on the edge of the specimens only, with no visible changes observed on the coating surface both under monotonic and cyclic loading until the final fracture.

Acknowledgment

The results presented in this paper were obtained within the project KomCerMet (Contract No. POIG.01.03.01-14-013/08-00 with the Polish Ministry of Science and Higher Education) in the framework of the Operational Programme Innovative Economy 2007-2013 and within the National Polish Project "Nanocomposite Ni-W/ZrO_2 coatings obtained by electrochemical deposition as an alternative to toxic chromium coatings—preparation, characterization and properties" under Grant Agreement No. NCN 2011/01/B/ST8/03974.

References

1. W.H. Safranek, *The Properties of Electrodeposited Metals and Alloys*, Elsevier, New York, 1974
2. L.J. Durney, *Electroplating Engineering Handbook*, Van Nostrand, Reinhold, 1984
3. A.S.M. Handbook, *Surface Engineering*, Vol 5, ASM International, Materials Parks, OH, 1994
4. E.W. Brooman, Corrosion Performance of Environmentally Acceptable Alternatives to Cadmium and Chromium Coatings: Chromium: Part I, *Met. Finish.*, 2000, **98**, p 38–43
5. M.P. Nascimento, R.C. Souza, I.M. Miguel, W.L. Pigatin, and H.J.C. Voorwald, Effects of Tungsten Carbide Thermal Spray Coating by HPHVOF and Hard Chromium Electroplating on AISI, 4340 High Strength Steel, *Surf. Coat. Technol.*, 2001, **138**, p 113–124
6. U. Wiklund, P. Hedenqvist, and S. Hogmark, Multilayer Cracking Resistance in Bending, *Surf. Coat. Technol.*, 1997, **97**, p 773–778
7. T. Yamasaki, High-Strength Nanocrystalline Ni-W Alloys Produced by Electrodeposition, *Mater. Phys. Mech.*, 2000, **1**, p 127–132
8. P. Indyka, E. Beltowska-Lehman, M. Faryna, and K. Berent, Microstructural and Microchemical Characterization of the Nickel-Based Thin Films Prepared by Electrodeposition, *Arch. Metall. Mater.*, 2010, **55**, p 421–427
9. T. Yamasaki, P. Schlossmacher, K. Ehrlich, and Y. Ogino, Formation of Amorphous Electrodeposited Ni-W Alloys and Their Nanocrystallization, *Nanostruct. Mater.*, 1998, **10**, p 375–388
10. T. Nasu, M. Sakurai, T. Kamiyama, T. Usuki, O. Uemura, and T. Yamasaki, EXAFS Study on Amorphous and Nanocrystalline M-W (M = Fe, Ni) Alloys Produced by Electrodeposition, *J. Non-Cryst. Solids*, 2002, **321–314**, p 319–322
11. C.A. Schuh, T.G. Nieh, and H. Iwasaki, The Effect of Solid Solution W Additions on the Mechanical Properties of Nanocrystalline Ni, *Acta Mater.*, 2003, **51**, p 431–443
12. D.B. Lee, J.H. Ko, and S.C. Kwon, High Temperature Oxidation of Ni-W Coatings Electroplated on Steel, *Mater. Sci. Eng. A*, 2004, **380**, p 73–78
13. H. Iwasaki, K. Higashi, and T.G. Nieh, Tensile Deformation and Microstructure of a Nanocrystalline Ni-W Alloy Produced by Electrodeposition, *Scripta Mater.*, 2004, **50**, p 395–399
14. H. Somekawa, T.G. Nieh, and K. Higashi, Instrumented Indentation Properties of Electrodeposited Ni-W Alloys with Different Microstructures, *Scripta Mater.*, 2004, **50**, p 1361–1365
15. M. Ma, V.S. Donepudi, G. Sandi, Y.K. Sun, and J. Prakash, Electrodeposition of Nano-Structured nickel-21% Tungsten Alloy and Evaluation of Oxygen Reduction Reaction in a 1% Sodium Hydroxide Solution, *Electrochim. Acta*, 2004, **49**, p 4411–4416
16. E.M.K. Hillier and M.J. Robinson, Permeation Measurements to Study Hydrogen Uptake by Steel Electroplated with Zinc-Cobalt Alloys, *Corros. Sci.*, 2006, **48**, p 1019–1035
17. K.P. Mroz and Z. Mroz, On Crack Path Evolution Rules, *Eng. Fract. Mech.*, 2010, **77**, p 1781–1807
18. K.P. Mroz and K. Dolinski, The Crack Growth Prediction in Homogeneous Materials and Bimaterial Systems, *ZAMM*, 2010, **90**, p 721–744
19. T. Hanlon, Y.N. Kwon, and S. Suresh, Grain Size Effects on the Fatigue Response of Nanocrystalline Metals, *Scripta Mater.*, 2003, **49**, p 675–680
20. K.R. Sriraman, S. Ganesh Sundara Raman, and S.K. Seshadri, Influence of Crystallite Size on the Hardness and Fatigue Life of Steel Samples Coated with Electrodeposited Nanocrystalline NiW Alloys, *Mater. Lett.*, 2007, **61**, p 715–771
21. A. Pertuz, J.A. Berrios, and E.S.P. Cabrera, Influence of a Commercial Electroless Ni-P Deposit on the Fatigue Properties of a Notched and Unnotched SAE 4140 Steel, *Surf. Coat. Technol.*, 2000, **72**, p 133–134
22. P. Indyka, E. Beltowska-Lehman, L. Tarkowski, A. Bigos, and E. García-Lecina, Structure Characterization of Nanocrystalline Ni-W Alloys Obtained by Electrodeposition, *J. Alloy. Compd.*, 2014, **590**, p 75–79
23. E. Beltowska-Lehman, P. Indyka, A. Bigos, M. Kot, and L. Tarkowski, Electrodeposition of Nanocrystalline Ni-W Coatings Strengthened by Ultrafine Alumina Particles, *Surf. Coat. Technol.*, 2012, **211**, p 62–66
24. J.W. Dini, *Electrodeposition. The Materials Science of Coatings and Substrates*, Noyes Publications, Westwood, 1993
25. A. Kutzelnigg, The Porosity of Electrodeposits, Causes, Classification and Assessment, *Plating*, 1961, **48**, p 382–387
26. D. Tabor, *Hardness of Metals*, Oxford University Press, Oxford, 1951
27. K.L. Johnson, The Correlation of Indentation Experiments, *J. Mech. Phys. Solids*, 1970, **18**, p 115–126
28. A.E. Giannakopoulos, P.-L. Larsson, and R. Vestergaard, Analysis of Vickers Indentation, *Int. J. Solids Struct.*, 1994, **31**, p 2679–2708
29. P.-L. Larsson, E. Soderlund, A.E. Giannakopoulos, D.J. Rowclife, and R. Vestergaard, Analysis of Berkovich Indentation, *Int. J. Solids Struct.*, 1996, **33**, p 221–248
30. P.L. Larsson, Investigation of Sharp Contact at Rigid Plastic Conditions, *Int. J. Mech. Sci.*, 2001, **43**, p 895–920
31. E.J. Pavlina and C.J. Van Tyne, Correlation of Yield Strength and Tensile Strength with Hardness for Steels, *J. Eng. Perform.*, 2008, **17**(6), p 888–893